

THE INFLUENCE OF THE ADDITION POSITION OF A TRACER ON CFD SIMULATED MIXING TIMES IN A VESSEL AGITATED BY A RUSHTON TURBINE

J.M. Bujalski, Z. Jaworski*, W. Bujalski and A.W. Nienow

The Centre for Formulation Engineering, School of Engineering, The University of Birmingham, UK

*Faculty of Chemical Engineering, Technical University of Szczecin, Szczecin, Poland

Previous papers on simulated mixing times in stirred vessels using CFD have sometimes given predictions in good agreement with empirical equations based on experiments and some have not. In this CFD study, mixing times have been determined for a vessel agitated by a Rushton turbine. The flow field was developed using the sliding mesh approach and computational parameters and the point of addition of the tracer have been varied. The simulations were very insensitive to the former whilst the radial distance from the wall of the latter had a very profound effect on both the mixing time and the development of the concentration field. When the addition point was close to the sliding mesh surface, the simulation was in good agreement with empirical predictions whilst that for a point close to the wall was much too long. This finding may explain the contradictions in the literature.

Keywords: stirred vessel, CFD, sliding mesh, mixing times, modelling

INTRODUCTION

When first attempted, the modelling of mixing times in stirred vessels used experimental LDV data as the boundary conditions for the impellers^{1,2}. The work showed that the simulated mixing times, t_m , could be different if the position of the addition point was varied axially. Lunden *et al.*³ implemented boundary conditions proposed by Kresta and Wood⁴ who used the original swirling radial jet model of Kolar *et al.*⁵ for investigating the influence of the radial position of the tracer addition and again found that the point of addition had a significant influence on t_m correlations. In the more recent work^{6,7}, such systems were modelled using the sliding mesh technique and, in general, showed very good agreement between CFD predicted t_m and experimental results. However, the position of the injection point, which had led to different t_m values with the earlier work, was not investigated.

For dual impellers, Jaworski *et al.*⁸ and Bujalski *et al.*⁹ showed that predicted t_m values based on sliding mesh simulations could be significantly different (by a factor of 2 to 3) from experiments. Recent results by Do *et al.*¹⁰ gave closer predictions of mixing times for dual Rushton turbines but the authors did not give a clear description of the method they used though it appeared to be the sliding mesh technique. Again, these authors did not investigate the influence on t_m of the radial position of the tracer addition point.

This paper investigates the influence of certain computational parameters and of the radial position of the addition point when using sliding mesh CFD on the simulated mixing times in the high transitional and turbulent flow regime. It concentrates on the computations for the high transitional regime because of the availability of experimental t_m values under these conditions for this geometry¹¹. However, the simulations were also performed for the fully turbulent case and gave the same general trend¹² though the results are not shown here.

MIXING TIME: DEFINITIONS AND EMPIRICAL CORRELATIONS

The t_{90} mixing time is defined as the time from the introduction of tracer to the time when the tracer concentration at the sensor position has reached and remains within a value of $\pm 10\%$ of the final value. An example of a sensor response and the t_{90} mixing time reading is shown in Figure 1. Analogous definitions and procedures lead to the t_{95} and t_{99} mixing times.

In order to quantitatively assess the accuracy of the predicted CFD mixing time simulations and to back up the experimental results¹¹, the simulations results were also compared with three different empirical literature correlations based on experimental data. Fasano and Penney¹³ proposed a general correlation for different impellers which can be used to calculate the mixing time for any level of uniformity, U, where $0 < U < 1$. Thus, when, for example, $U=0.9$, t_m is the 90% mixing time, t_{90} . For a Rushton turbine, equation (1) applies:

$$t_U = \frac{-\ln(1-U)}{1.06 \times \left(\frac{D}{T}\right)^{2.17} \left(\frac{T}{H}\right)^{0.5}} \quad (1)$$

Thus, values of mixing times can be estimated for different levels of uniformity. Bakker and Fasano¹⁴ found that their CFD simulations fitted predictions from equation (1) very well for U values of 0.9 and higher. Cooke *et al.*¹⁵ proposed a general correlation for t_{90} , applicable for $Re > 5000$ and mixing vessels of aspect ratio up to 3, particularly for multiple radial flow impellers. For a single radial flow impeller system in vessel of $H=T$, the correlation becomes:

$$t_{90} = 3.3 \left(\frac{1}{N}\right) (Po)^{-1/3} \left(\frac{T}{D}\right)^{2.43} \quad (2)$$

Ruszkowski¹⁶ proposed a general relationship for single radial or axial flow impeller for t_{95} in equation (3) which is applicable for $Re > 6400Po^{-1/3}$:

$$t_{95} = 5.9T^{2/3} \left(\frac{\rho V}{P}\right)^{1/3} \left(\frac{T}{D}\right)^{1/3} \quad (3)$$

METHODS AND MATERIALS

EXPERIMENTAL

The mixing times were measured using the decolorisation of starch/iodine solution with the addition of sodium thiosulphate¹¹ in a $T=H=0.22$ m vessel with four equally spaced baffles (width $B=0.1T$) (see Figure 2). A standard Rushton turbine of the diameter $D=0.46T$ placed at a height $C=0.33T$ was used with the material of the disk and blades of thickness x giving $x/D=0.0328$. The agitation speed was 50 rpm and power and torque were determined by an air bearing/load cell technique. Additions were made at the top, middle and bottom of the tank and at each level, three repeats were undertaken.

VESSEL GEOMETRY

A commercial CFD software CFX 4.3 (AEA Technology™) was used in the geometry creation and to predict the flow field and mixing times. The impeller was modelled in the simulated geometry as the source of the momentum, rotating in a clockwise direction, with infinitely thin walls, using the sliding mesh method. The sliding mesh boundary was positioned half way between the blade tip and the end of the baffles. The vessel had no symmetry boundary as the tracer distribution was non-symmetrical and so the whole 360° geometry had to be simulated using around 130000 cells ($I=45$; $J=33$; and $K=88$), see Figure 3.

FLOW FIELD

The flow field was modelled using 88 time steps per impeller revolution with 1 cell in the tangential direction for each time step with 30 iterations per time step. Overall 15 revolutions at the impeller speed of 50 rpm were simulated to get the flow field which was used in the initial mixing time simulations. The fluid modelled had the properties of water. Since the experimental flow regime was in the high transitional Reynolds number range ($Re=8600$), a low Reynolds number turbulence model was used in the simulation. To reduce the risk of divergence in the solution due to the large number of blocks and complex geometry, the hydrodynamic equations were solved using a general AMG solver as recommended by AEA Technology¹⁷. In the simulation of the flow field using the sliding mesh approach, the total, normalised residuals decreased to the value of 10^{-3} which is considered acceptable for this type of flow simulations¹⁸.

From the analysis of the flow field, the power number was calculated¹⁹ from the pressures and shear stresses converted into forces and hence the torque acting on the impeller surfaces.

MIXING TIMES

The mixing times were simulated using an inert tracer that was added at a point in the first cell just below the liquid surface at an angle of 60° from a baffle (see Figure 4). Four radial distances were used and all were in the stationary part of the mesh (see Figure 4). Point 1 was close to the vessel wall (3rd computational cell), point 2 (7th computational cell) was just in the “shadow” of the baffle, point 3 (8th computational cell) was just outside the baffle ‘shadow’ and point 4 was positioned next to the sliding mesh boundary (11th cell from the vessel wall).

Nine sensors were simulated in order to follow the concentration of the added tracer (see Figure 2). Their location was based on the work of Otomo²⁰. Four sensors (numbers 1 to 4) were located in front of the four baffles and an additional four sensors (5 to 8) were placed between the baffles, all at the same height of 0.11m above the impeller centreline. Sensor 9 was positioned in front of a baffle and below the impeller centreline at an axial distance of 0.04m. All the sensors were in the stationary mesh and the concentration variation with time was predicted for each sensor at each simulated time step.

Two modelling methods were employed to obtain the mixing times. In the first method¹⁸, when the tracer was added, the hydrodynamic equations were ‘frozen’ by deactivating the solver for momentum transfer. Thus, only the distribution of the tracer in time was predicted at each sensor using the scalar transport equation (4).

$$\frac{\partial}{\partial t}(\rho Y_i) + \nabla \cdot (\rho u Y_i) = \nabla \cdot \left(\left(\Gamma_i + \frac{\mu_T}{Sc_T} \right) \nabla Y_i \right) \quad (4)$$

In equation (4), Y_i and Γ_i are the mass fraction and molecular diffusion coefficient of species i , respectively. Sc_T is the turbulent Schmidt Number and was set to the default value of 0.9. The tracer fluid had the same properties as the bulk fluid used. The simulations were run for 90 seconds to ensure that the tracer was uniformly distributed throughout the volume. In practice, uniformity was achieved after 50 seconds even in the extreme case.

In the second approach, the hydrodynamic equations were solved concurrently with the tracer distribution in order to model the variation of the velocity field with the passing of the impeller blades in front of the stationary baffles. In order to cope with the extra computational demands in the simulation, the probe responses were run for 60 seconds. In all the cases, the simulated responses reached a plateau well within the time allowed (Figure 1 is an example for sensor 4).

The size of time step in the mixing time simulations for both methods was also investigated and the optimum value, in terms of CPU time needed to run the mixing time simulation was established. Thus, 8 tangential cells per time step were used in all simulations ensuring the comparability of the results. All the normalised sensor concentration responses, I_s , (equation (5)), were related to the final concentration, C_T , whilst the initial concentration C_0 was zero in all simulations.

$$I_s = \frac{|C_i - C_0|}{C_T - C_0} = \frac{C_i}{C_T} \quad (5)$$

To check the mass balance, the mass of the tracer was integrated, at each time step, over the whole stirred vessel volume. It was found that the value of the tracer mass did not change significantly. In the simulation of the tracer distribution for the mixing time, the residuals of the tracer reduced in 30 iterations to a value of 10^{-5} from the second to the last iteration. Thus, the solution was considered converged for each mixing time simulation.

RESULTS AND ANALYSES

POWER NUMBER

A power number of $Po=4.2$ was obtained from the simulation. This value corresponds very well with the value of 4.3 obtained from the correlation proposed by Bujalski *et al.*²¹ which relates the power number to the minor dimensions of the impeller such as blades and disk thickness and also to the scale of operation.

MIXING TIMES

Experimental vs. empirical correlations

The experimental results obtained by decolorisation¹¹ gave the same mixing time (within $\pm 5\%$) regardless of the addition point. This value is compared with the three empirical correlations^{13,15,16} in Table 1.

Table 1 Mixing times experiments and literature correlations (equations 1, 2 and 3)

| Mixing times | Experiment ¹¹ [s] | Equation 1 [s] | Equation 2 [s] | Equation 3 [s] |
|--------------|------------------------------|----------------|----------------|----------------|
| t_{90} | 13 | 14 | 13 | - |
| t_{95} | - | 18 | - | 18 |
| t_{99} | - | 28 | - | - |

For equation (2), Po was obtained from the experimental work¹¹ whilst for equation (3), the power used was obtained from the present CFD simulations. The experimental value is very close to t_{90} calculated from equations (1) and (2) which is consistent with the work of Otomo²⁰ who found that t_{90} obtained from sensor responses was similar to t_m by decolorisation.

Simulation vs. empirical correlations

Computational Parameters:

The transients were simulated initially for the tracer addition point 1 using 8 tangential cells per time step and all the simulations, except where stated, were performed using the flow field established after 15 impeller revolutions. One feature seen in the simulated sensor responses

(Figure 1) is that all are smooth i.e. unlike experimental data, there is no interference or ‘noise’. Subsequently, the simulated mixing times (t_{90} , t_{95} and t_{99}) were calculated from the average of the nine individual sensor responses and the values obtained are compared with values from equation (1) and the experimental result¹¹ in Figure 5. It can be clearly seen that the simulation results were over predicting all the mixing times (on average by a factor of ~ 2). Initially, the problems was thought to be related to the use of 8 cells per time step which might have been too large so that the fine fluctuations in the sensor response were missed. Therefore simulations with 2 cells per time step were tried but this change was found not to have a great influence (again see Figure 5). However, it should be noted that for both time steps, the simulation results showed the same trend.

It was also considered that the over estimation of the mixing times might be due to the use of a frozen flow field in the simulation, as this form of simulation does not take into account the variation in the flow as the impeller blade passes in front of the baffle. To see the effect that the hydrodynamic equations have on the mixing times, the simulation was run with the hydrodynamic equations being solved simultaneously with that for the tracer distribution. Figure 6 shows the predictions with and without the hydrodynamic equations activated. Clearly, this concurrent approach has not reduced the discrepancy. Again the size of the time step was decreased but it did not improve the agreement. It should be noted that the computational demands of this approach were about 10 times greater than those when the flow field was frozen.

To see the influence of the development of the flow field, the simulation were also performed using flow fields developed after 5 or 10 impeller revolutions. In these simulations, the tracer was added again at point 1 and the predictions of t_{90} , t_{95} and t_{99} have been compared with equation (1) in Figure 7. For the first two levels of homogenisation, i.e. 90% and 95%, the mixing times are not significantly affected by the different initial flow fields.

Effect of Feed Location

Since changes in computational strategy made so little difference to the simulations, it was also decided to investigate the impact of the point of feeding especially since earlier publications without sliding mesh have shown a sensitivity to this parameter. The position of addition was changed initially to point 4 (see Figure 4) and simulations were again carried out with 8 tangential cells per time step and 30 iterations per time step. The simulations using the new addition point gave dramatically better agreement with the literature correlation predictions and experimental data (see Table 2). It is particularly noteworthy that in the experimental work¹¹, many addition points were used and all gave essentially the same mixing time.

Table 2 Influence of addition point on the simulated mixing time in comparison with equation (1) and experimental data

| Mixing times | Experiment ¹¹ [s] | Equation 1 [s] | | Point 1 | | Point 4 | |
|--------------|------------------------------|----------------|--------------------|-----------------|--------------------|-----------------|--------------------|
| | | Mixing time[s] | Ratio t_m/t_{90} | Mixing time [s] | Ratio t_m/t_{90} | Mixing time [s] | Ratio t_m/t_{90} |
| t_{90} | 13 | 14 | 1.0 | 28 | 1.0 | 13 | 1.0 |
| t_{95} | - | 18 | 1.3 | 33 | 1.15 | 17 | 1.3 |
| t_{99} | - | 28 | 2.00 | 46 | 1.64 | 25 | 1.9 |

An interesting aspect arising from the simulations is an analysis of the ratios of the mixing times at the different homogenisation levels, i.e., t_{90} , t_{95} and t_{99} , normalised with t_{90} . The values of the ratios are also given in Table 2 for the two addition points used in the simulation. For point 1, the mixing time ratios are completely different to the ratios from equation (1) whilst when the tracer is added at point 4, the ratios are very similar. This result shows that when the simulation data for t_{90} is close to the empirical value predicted from equation (1), then the simulation data can be used to extrapolate mixing times for different levels of homogenisation.

Simulations at points 2 and 3 (see Figure 4) were also undertaken using the same computational parameters as led to Figure 7 and Table 2 and the predictions are given in Figure 8. Clearly, at each level of homogeneity, the mixing time decreases steadily as the addition point moves from the wall towards the middle of the vessel, typically by a factor of about 2 with the value nearest the center being closest to the value from experiment and equation (1). Thus, the radial distance of the tracer addition point from the vessel wall has a great influence on the predicted mixing times.

Effect of sensor position

Ruszkowski¹⁶ for $Re > 6400Po^{-1/3}$ and Thyn *et al.*²² and Rielly and Pandit²³ for turbulent conditions have all shown experimentally that the mixing time measured by the conductivity technique does not change significantly for a single impeller system with the variation of the sensor position. Here, in all the cases, the CFD-predicted mixing time depended on the location of the sensor. Figure 9 is given as an example of the differences for t_{90} , t_{95} and t_{99} for all 9 probes for addition at the extreme addition points 1 and 4. At each position, there is a large scatter with the greatest occurring with t_{99} at addition point 1. Sensor 9 was the only sensor positioned below the impeller but it did not give results consistently different from the other sensors.

COMPUTATIONAL VISUALISATION

To investigate the reason for such differences in the simulated mixing times for different radial feed positions, CFX Analyse visualisation software was used to obtain 3-dimensional images of iso-concentration fields. Such images (Figure 10 and 11) clearly show the predicted spread of the tracer through the vessel. The iso-concentrations fields shown in Figure 10 and 11 have arbitrary values normalised with the tracer injection concentration, chosen to help in the visualisation of the 3D distribution of the tracer.

Figure 10a shows the concentration field just after tracer addition (at the first time step in the simulation) at point 1 close to the wall. The larger plume is of the lower tracer concentration (blue, 0.009), whilst the smaller (red, ~ 1.0) is still very close to the feed concentration and also indicates the position of the tracer addition. Figure 10b is of the tracer plume after 10 impeller revolutions. Two levels of concentration are shown for clarity, a green plume of higher concentration (0.006) and a blue of lower concentration (0.002). It is very clear that the tracer plume has not moved greatly in the radial direction and only slightly in the tangential one. The plume is still confined mostly to the quarter of the vessel where the injection of the tracer occurred as though its movement is 'shielded' by the presence of the baffles.

In Figure 11, the tracer addition was at position 4 shown in green (concentration ~ 1.0) close to the sliding mesh boundary in Figure 11a. In this first time step in the simulation, the tracer plume (blue, 0.001) has already started to move in the tangential direction against the rotation of the impeller. This phenomena of reverse flow has been already reported by Jaworski *et al.*¹⁸ for FluentTM software and is probably a characteristic feature of the sliding mesh method. After 10 revolutions of the impeller (Figure 11b), the tracer plume has split into

two regions shown clearly by the blue iso-surfaces of ratio 0.002. The first region is in the stationary mesh, which is similar to that in Figure 10, being confined to the volume between the two baffles where the addition of the tracer was made. In addition, in the rotating mesh (second region), the tracer is spread evenly in the tangential direction and has moved axially downwards towards the top of the impeller. Thus, the rotating mesh in the simulation appears to be promoting the tangential and the axial distribution of the tracer plume and hence reducing the mixing time for point 4 additions compared to point 1. It may also account for why sensor 9 which is beneath the impeller gives the shortest mixing times for t_{95} and t_{90} in Figure 9.

When comparing Figure 10 and Figure 11 tracer distributions, it is clearly seen that the inner rotating mesh volume, which modelled the rotating impeller, was the main promoter of the distribution of the tracer. The closer the tracer addition point was to the sliding mesh boundary (see Figure 2), the faster the tracer was incorporated into that region and then distributed around the tank volume leading to shorter simulated mixing times (see Figure 8).

Lunden *et al.*³, who modelled a stirred tank using a stationary mesh geometry and experimental boundary conditions for the impeller flow, also found that the mixing time depended on the feed point. However, they suggested that the major factor was the lack of the tangential exchange of the tracer between the velocity flow loops which were in between the baffles. Thus, though the effect was similar to that found in this work including overpredicting mixing times, the underlying reasons appear to be quite different.

DISCUSSION AND CONCLUSIONS

Mixing times have been predicted using CFD with a sliding mesh approach for the modelling. Three different parameters were investigated. The first two, which were particularly concerned with the modelling strategy, involved the interaction between the flow field and the development of the concentration field and the size of the time step. The third concerned the mode of mixing, namely the impact of the tracer feed position at the top surface. The first two had little effect but surprisingly, contrary to experimental studies, the position of the feed point was very important. The great influence of the feed point was shown to be related to its position relative to the sliding mesh boundary and how the concentration field developed. This sensitivity led to some predictions being close to experimental results and empirical equations (all of which were themselves in good agreement) whilst others were much greater. This sensitivity to the feed point position when modelling which is not found experimentally may explain why CFD predictions in the literature have sometimes been in good agreement with experimental values and some have not. These results are also important because if CFD predictions of mixing time and the process of homogenisation are so sensitive to feed position when in practice they are not, the implications are also very serious for more complex processes such as competitive reactions and precipitation.

NOMENCLATURE

| | | |
|-------|-------------------------------------|----------------------|
| B | baffle width | [m] |
| C | impeller clearance | [m] |
| C_i | instantaneous tracer concentration | [kg/m ³] |
| C_T | terminal tracer concentration | [kg/m ³] |
| C_0 | initial tracer concentration | [kg/m ³] |
| D | impeller diameter | [m] |
| H | tank height | [m] |
| IS | tracer mixing index | [-] |
| I | number of cells in axial direction | [-] |
| J | number of cells in radial direction | [-] |

| | | |
|-----------------|---|----------------------|
| K | number of cells in tangential direction | [-] |
| N | impeller speed | [s ⁻¹] |
| P | impeller power | [W] |
| Po | Power Number | [-] |
| Re | Reynolds Number | [-] |
| Sc _T | turbulent Schmidt Number | [-] |
| T | tank diameter | [m] |
| t | time | [s] |
| U | degree of uniformity | [-] |
| u | velocity | [m/s] |
| V | volume | [m ³] |
| x | impeller blade thickness | [m] |
| Y _i | mass fraction | [kg/m ³] |

Greek symbols

| | | |
|----------------|-----------------------------------|----------------------|
| μ _T | turbulent viscosity | [kg/ms] |
| ρ | density | [kg/m ³] |
| Γ _i | molecular diffusivity of tracer i | [kg/ms] |

Subscripts

| | |
|------------|---|
| m | general mixing time |
| 90, 95, 99 | 90% 95% and 99% mixing times respectively (see Fig. 1 and text) |

ACKNOWLEDGEMENTS

One of the authors (JMB) would like to acknowledge the financial support of EPSRC and the Department of Chemical Engineering. The support of the Dr. Paul Hatton from the High Performance Computing Service at the University of Birmingham is acknowledged.

ADDRESS (CORRESPONDING AUTHOR)

Correspondence concerning this paper should be addressed to Dr. Waldemar Bujalski, The Centre for Formulation Engineering, School of Engineering, The University of Birmingham, Edgbaston, Birmingham B15 2TT, UK. Email: W.Bujalski@bham.ac.uk

FIGURES

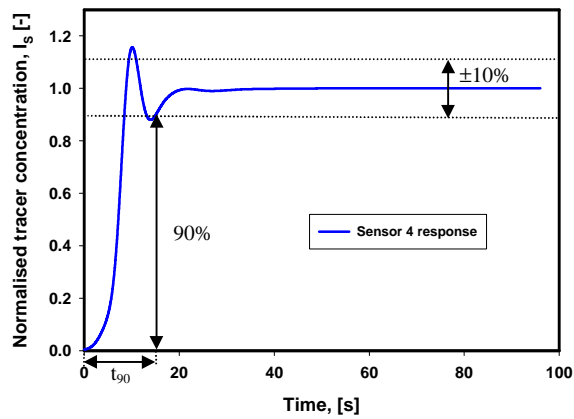


Figure 1 A graphical representation of t_{90} mixing time using the normalised simulated concentration response at sensor 4 as an illustration.

CFX

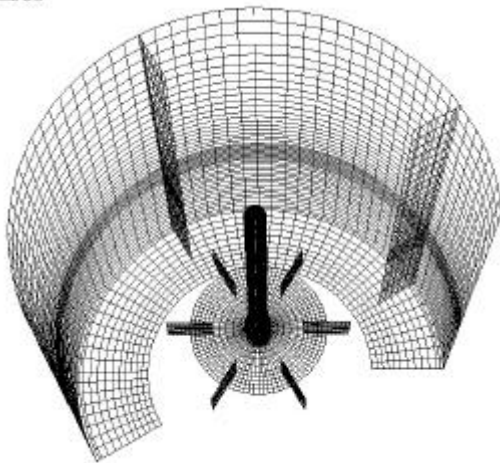


Figure 3 The mesh geometry used in the mixing times simulations.

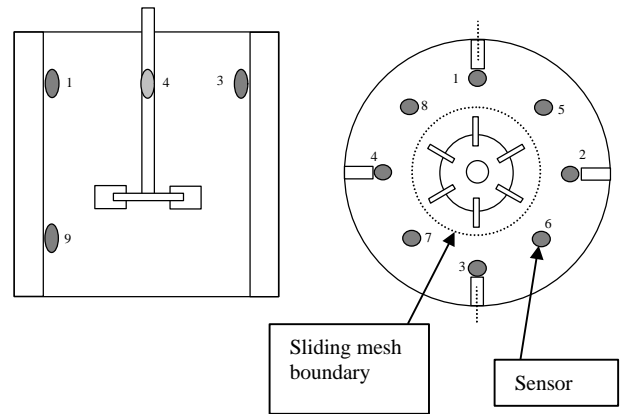


Figure 2 Schematic diagram of the experimental geometry showing the position of the sensors and the sliding mesh boundary.

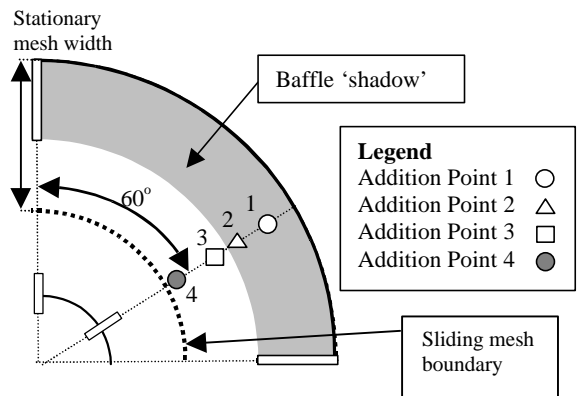


Figure 4 Schematic diagram of top of the vessel showing the position of the four tracer addition points.

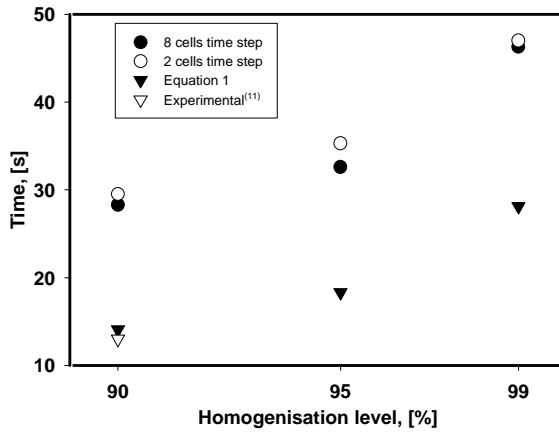


Figure 5 Influence of the size of the simulation time step on the predicted mixing time and a comparison with equation (1) and experimental data.

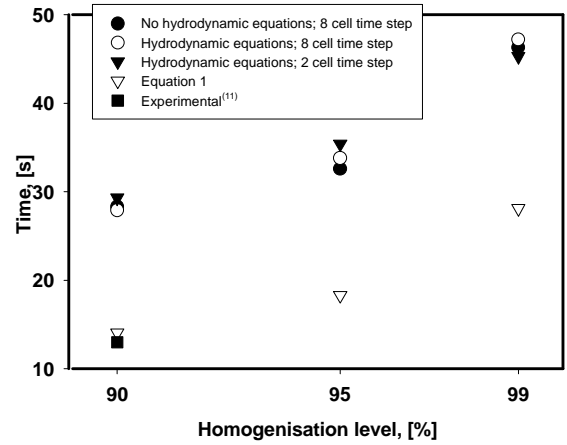


Figure 6 Comparison of mixing times calculated in parallel with the hydrodynamic equations using two different time step sizes with other cases.

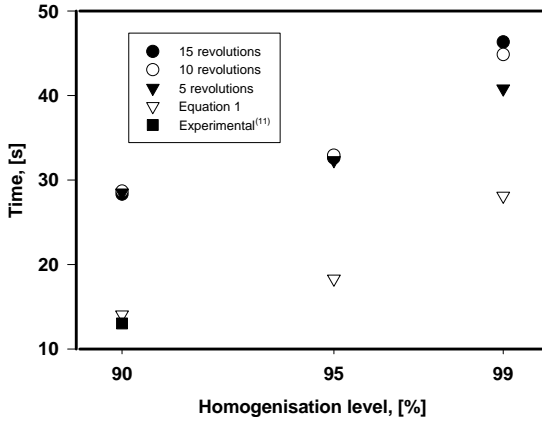


Figure 7 Mixing time as a function of the initial flow field development (impeller revolutions) in comparison with equation (1) and experimental data.

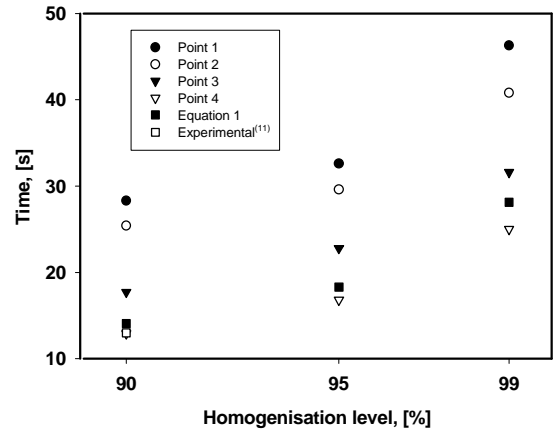


Figure 8 Influence of the position of tracer addition on the mixing: time comparison with equation (1) and experimental data.

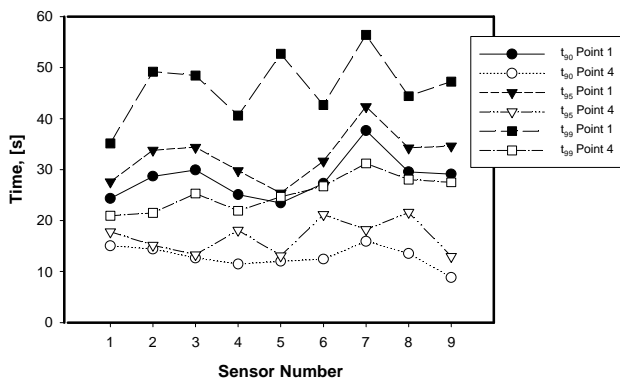
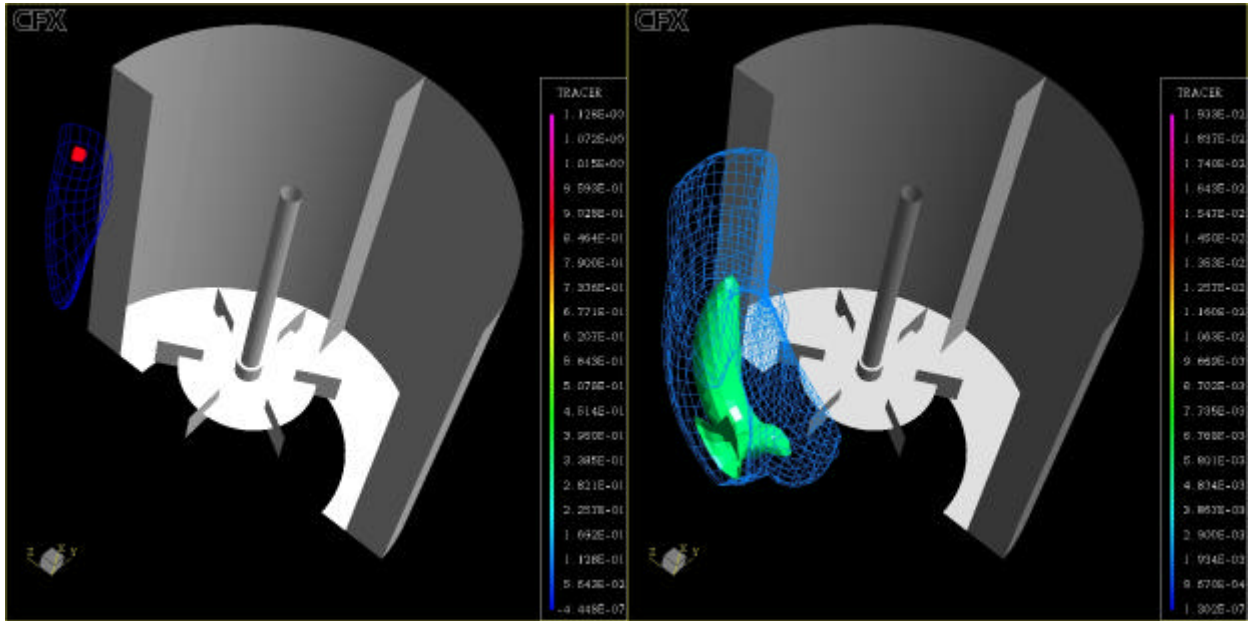


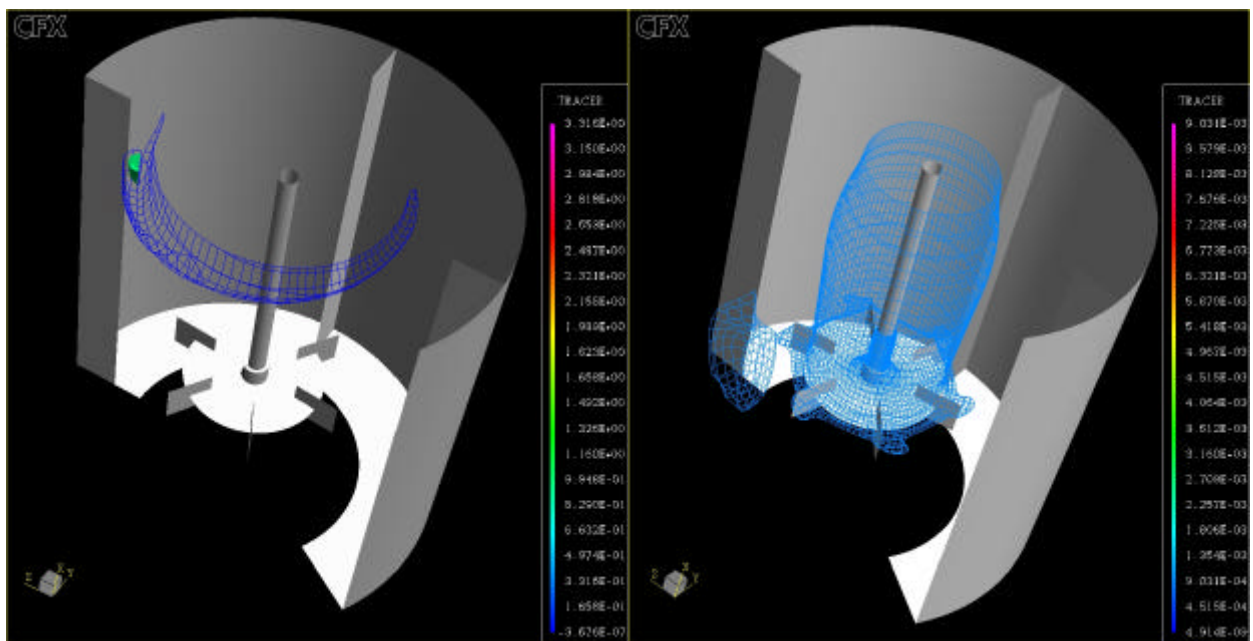
Figure 9 Mixing times at the nine sensors for addition at points 1 and 4.



a) Initial (after 1 time step)

b) After 10 revolutions of the impeller

Figure 10 The predicted tracer distribution after addition at point 1.



a) Initial (after 1 time step)

b) After 10 revolutions of the impeller

Figure 11 The predicted tracer distribution after addition at point 4.

REFERENCES

1. Ranade, V. V., Bourne, J. R. and Joshi, J. B., 1991, Fluid mechanics and blending in mechanically agitated tanks, *Chemical Engineering Science*, 46: 1883-1893.
2. Jaworski, Z., 1991, Makromieszanie w mieszalnikach cieczy (Macromixing in stirred tanks), *DSc Thesis*, (Warsaw University of Technology, Poland).
3. Lunden, M., Stenberg, O. and Anderson, B., 1995, Evaluation of a method of measuring mixing time using numerical simulation and experimental data, *Chemical Engineering Communications*, 139: 115-136.
4. Kresta, S. M. and Wood, P. E., 1991, Prediction of the three-dimensional turbulent flow in stirred tanks, *AIChE Journal*, 37: 448-460.
5. Kolar, V., Filip, P. and Curev, A. G., 1982, Swirling radial jet, *Applied Scientific Research (The Hague)*, 39: 329-335.
6. Jaworski, Z. and Dudczak, J., 1998, CFD modelling of turbulent macromixing in stirred tanks. Effect of the probe size and number on mixing indices, *Computers & Chemical Engineering*, 22: S293-S298.
7. Zhu, J. M., Mahmud, T. and Javed, K. H., 2001, Computational modelling of turbulent mixing in a batch agitated vessel, *6th World Congress of Chemical Engineering*, Melbourne, Australia.
8. Jaworski, Z., Bujalski, W., Otomo, N. and Nienow, A. W., 2000, CFD study of homogenization with dual Rushton turbines - comparison with experimental results. Part I: Initial studies, *Transactions of the Institution of Chemical Engineers*, 78: 327-333.
9. Bujalski, W., Jaworski, Z. and Nienow, A. W., 2002, CFD study of homogenization with dual Rushton turbines - Comparison with experimental results part II: MFR studies, *Transactions of the Institution of Chemical Engineers*, 80: 97-104.
10. Do, J. H., Shang, L. A., Kim, D. H. and Chang, H. N., 2001, Effect of impeller clearance on flow structure and mixing in bioreactor with two-stage impellers, *Engineering Life Science*, 5: 181-185.
11. Nienow, A. W. and Inoue, K., 1993, A study of precipitation: mixing, size distribution and morphology, *CHISA*, Paper H.9.4, Prague, Czech Republic.
12. Bujalski, J. M., 2002, CFD modelling of batch precipitation, *PhD Thesis*, (University of Birmingham, UK) (To be published).
13. Fasano, J. B. and Penney, W. R., 1991, Avoid blending mix-ups, *Chemical Engineering Progress*, 87: 56-63.
14. Bakker, R. A. and Fasano, J. B., 1994, Time dependent, turbulent mixing and chemical reaction in stirred tanks, *AIChE Symposium Series*, 90,: 71-77.
15. Cooke, M., Middleton, J. C. and Bush, J. R., 1988, Mixing and mass transfer in filamentous fermentations, *Proc. 2nd Int. Conf. on Bioreactor Fluid Dynamics*, King, R., 37-64, Cranfield, UK.
16. Ruskowski, S., 1994, A rational method for measuring blending performance and comparison of different impeller types, *Proc. 8th European Conference on Mixing*, 283-291, Cambridge, UK.
17. AEA Technology, 1995, CFX 4.1: User Manual.
18. Jaworski, Z., Bujalski, W., Otomo, N. and Nienow, A. W., 1999, CFD study of homogenisation with dual Rushton turbines - Comparison with experimental results, (146),: 81-91, Bradford, UK.
19. Jaworski, Z., Wyszynski, M. L., Moore, I. P. T. and Nienow, A. W., 1997, Sliding mesh computational fluid dynamics - a predictive tool in stirred tank design, *Proceedings of the Institution of Mechanical Engineers Part E- Journal of Process Mechanical Engineering*, 211: 149-156.
20. Otomo, N., 1996, A study of mixing with dual radial and dual axial flow impellers: blending and power characteristics, *PhD Thesis*, (University of Birmingham, UK).
21. Bujalski, W., Nienow, A. W., Chatwin, S. and Cooke, M., 1987, The dependency on scale of power numbers of Rushton disc turbines, *Chemical Engineering Science*, 42: 317-326.
22. Thyn, J., Novak, V. and Pock, P., 1976, Effect of the measured volume size on the homogenisation time, *Chemical Engineering Journal*, 12: 211-217.
23. Rielly, C. D. and Pandit, A. B., 1988, The mixing of Newtonian liquids with large density and viscosity differences in mechanically agitated contactors, *6th European Conference on Mixing*, 69-74, Pavia, Italy.